Low-Temperature-Induced Structural Changes in the Apo Regulatory Domain of Skeletal Muscle Troponin C[†,‡]

Sakae Tsuda,*[,§] Ai Miura,[§] Stéphane M. Gagné,[||] Leo Spyracopoulos,[||] and Brian D. Sykes[||]

Bioscience and Chemistry Division, Hokkaido National Industrial Research Institute (HNIRI), Toyohira-ku, Sapporo 062-8517, Japan, and Department of Biochemistry, Medical Research Council Group in Protein Structure and Function, University of Alberta, Edmonton, Alberta T6G 2H7, Canada

Received December 15, 1998; Revised Manuscript Received March 4, 1999

ABSTRACT: Contractile activity of skeletal muscle is triggered by a Ca^{2+}-induced "opening" of the regulatory N-domain of troponin C (apo-NTnC residues 1−90). This structural transition has become a paradigm for large-scale conformational changes that affect the interaction between proteins. The regulatory domain is comprised of two basic structural elements: one contributed by the N-, A-, and D-helices (NAD unit) and the other by the B- and C-helices (BC unit). The Ca^{2+}-induced opening is characterized by a movement of the BC unit away from the NAD unit with a concomitant change in conformation at two hinges (Glu^{41} and Val^{65}) of the BC unit. To examine the effect of low temperatures on this Ca^{2+}-induced structural change and the implications for contractile regulation, we have examined nuclear magnetic resonance (NMR) spectral changes of apo-NTnC upon decreasing the temperature from 30 to 4 °C. In addition, we have determined the solution structure of apo-NTnC at 4 °C using multinuclear multidimensional NMR spectroscopy. Decreasing temperatures induce a decrease in the rates and amplitudes of pico to nanosecond time scale backbone dynamics and an increase in α-helical content for the terminal helices of apo-NTnC. In addition, chemical shift changes for the H_α resonances of Val^{65} and Asp^{66}, the hinge residues of the BC, unit were observed. Compared to the solution structure of apo-NTnC determined at 30 °C, the BC unit packs more tightly against the NAD unit in the solution structure determined at 4 °C. Concomitant with the tighter packing of the BC and NAD structural units, a decrease in the total exposed hydrophobic surface area is observed. The results have broad implications relative to structure determination of proteins in the presence of large domain movements, and help to elucidate the relevance of structures determined under different conditions of physical state and temperature, reflecting forces ranging from crystal packing to solution dynamics.

Contractile activity in striated muscle is regulated by troponin C (TnC[1]), a Ca^{2+}-binding subunit of troponin located on actin filaments together with two other subunits, troponin I (TnI) and troponin T (TnT). TnC is a small acidic protein (18 kDa) consisting of two similarly sized globular domains, the N-terminal domain (NTnC) and the C-terminal domain (CTnC). The domains contain two Ca^{2+}-binding sites each. The Ca^{2+}-binding sites in CTnC are saturated at physiological Ca^{2+} concentrations; thus, NTnC is thought to be responsible for regulation of muscle contraction via binding of Ca^{2+}. The binding of Ca^{2+} induces a conformational change in NTnC so as to cancel the inhibitory activity of TnI. The structural change in NTnC is then transmitted to the actin filament through TnT. This succession of protein structural changes leads to formation of the Mg^{2+}-activated ATPase actomyosin complex, and ultimately results in muscle contraction (*1*−*5*).

TnC isoforms and related contractile mechanisms have been identified in striated muscle in a variety of vertebrates and invertebrates whose environments have temperatures ranging from 4 to 41 °C. These organisms include rabbit, chicken, frog, carp, shark, sea squirt, lobster, crayfish, barnacle, lethocerus, horseshoe crab, and scallop (*6*−*17*). It is believed that ectothermic species such as scallop, whose habitat is cold seawater, experience the lowest temperature of 4 °C, while chicken striated muscle experiences the highest temperature of 41 °C (*18*). Hence, one can assume that the Ca^{2+}-dependent regulatory function of TnC is conducted at low temperatures. A detailed structural understanding of the molecular architecture of a protein at low temperatures would provide valuable insight into its function. For example, the cold-adapted enzymes produced from psychrophilic and psychrotrophic microorganisms possess high catalytic efficiency at low temperatures (∼0 °C) and exhibit rapid inactivation at temperatures as low as 30 °C, and thus offer

[†] This research was supported by the Medical Research Council of Canada and the Protein Engineering Network Center of Excellence (PENCE).

[‡] The atomic coordinates for the final structures and the sets of restraints have been deposited with the Brookhaven Protein Data Bank (file names 1SKT and 1ZAC).

* To whom correspondence should be addressed. E-mail: tsuda@hniri.go.jp. Phone: +81-11-857-8912. Fax: +81-11-857-8983.

[§] Hokkaido National Industrial Research Institute (HNIRI).

[||] University of Alberta.

[1] Abbreviations: TnC, troponin C; NTnC, N-domain of TnC; CTnC, C-domain of TnC; apo-NTnC, NTnC in the Ca^{2+}-free state; 2Ca-E41A-NTnC, E41A mutant of NTnC with 2 mol of Ca^{2+} bound; CaM, calmodulin; HLH, helix−loop−helix; NMR, nuclear magnetic resonance; NOE, nuclear Overhauser enhancement; rmsd, root-mean-square deviation; SA, simulated annealing; CSI, chemical shift index.

10.1021/bi982936e CCC: $18.00
Published on Web 04/16/1999

great potential in biotechnological applications (*19*). However, the molecular basis of cold adaptation in proteins is unclear due to the lack of studies on structural and dynamic changes of a protein in solution induced by a reduction in temperature.

This study focuses on chicken skeletal muscle NTnC in monitoring low-temperature-induced changes because of a large body of structural and dynamic data at normal temperature (~30 °C) exists. This structural database includes X-ray crystal structures of whole TnC where NTnC is in the apo form while CTnC is in the Ca^{2+}-saturated form (*20*, *21*), the Herzberg−Moult−James model for the Ca^{2+}-induced structural change in NTnC (*22*), the NMR structure of a TR_1C fragment (NTnC without the N-terminal helix) in the apo form (*23*), the NMR structures of NTnC in both the apo and Ca^{2+} states (*24*), the NMR structure of intact TnC in the $4Ca^{2+}$ form (*25*), the NMR structure of the E41A mutant of NTnC in the $2Ca^{2+}$ form (*26*), and the X-ray structure of NTnC in the $2Ca^{2+}$ form (*27*). In addition, the X-ray structure of rabbit skeletal muscle TnC which is 90% homologous in primary structure with chicken TnC has recently been determined in two different crystal forms (*28*). The detailed backbone and side chain dynamics of apo-NTnC have also been studied at 30 °C via heteronuclear ^{15}N and ^{2}H NMR relaxation measurements (*29*). The structural studies reveal that NTnC is composed of five helices: N-, A-, B-, C-, and D-helices where the A- and B-helices flank Ca^{2+}-binding site I and the C- and D-helices flank Ca^{2+}-binding site II. The Ca^{2+}-binding sites are composed of two paired helix−loop−helix (HLH) calcium binding motifs, as found in a variety of the proteins of the calmodulin superfamily. The N-, A-, and D-helices form a structural unit (NAD unit), and the B- and C-helices form another unit (BC unit) which includes a flexible linker. The main hydrophobic core of NTnC is formed at the interface of these structural units. The binding of Ca^{2+} to skeletal NTnC causes a movement of the BC structural unit away from the NAD unit. The structural "opening" of NTnC accompanying the movement of the BC unit is concomitant with large changes in the dihedral angles at two "hinges" located at the beginning (Glu^{41}) and the end (Val^{65}) of this unit; that is, the BC unit is a "door" equipped with these two hinges. The opening of NTnC leads to the exposure of a large hydrophobic surface (*25*). The side chains which are exposed in the Ca^{2+}-induced opening of NTnC show restricted mobility in the "closed" or apo state (*29*). It has been proposed that a gain in conformational entropy for these side chains upon the opening of NTnC may offset the free energy cost for exposing hydrophobic groups (*30*). A similar, much smaller, Ca^{2+}-induced structural opening has also been identified in cardiac NTnC, where the BC unit moves slightly away from the NAD unit (*29*). Such a Ca^{2+}-induced opening of the BC unit door allows the interaction between the exposed hydrophobic surface and TnI, leading to the cancellation of the inhibitory action of TnI (*24*). Hence, the change in the orientation of the BC unit relative to the NAD unit is an essential mechanism of contractile regulation in NTnC.

Recently, Foguel et al. (*31*) monitored fluorescence changes of a tryptophan probe at residue 29 of chicken skeletal muscle NTnC (F29W mutant). They proposed that a decrease in temperature under high pressure (2.2 kbar) gives rise to a conformational opening in the molecule, analogous to the Ca^{2+}-induced opening (*31*). It was also found that the change in fluorescence intensity is small when temperature alone is decreased at atmospheric pressure. A low-temperature-induced increase in the apparent Ca^{2+} affinity was also pointed out (*31*). The study presented here focuses on the effect of low temperatures on a protein at atmospheric pressure (1 bar) to avoid a high-pressure-induced opening or denaturation of apo-NTnC. NMR spectroscopy is ideally suited for studying changes in structure and dynamics of a protein on a per residue basis and under a variety of physicochemical conditions (temperature, pH, ionic concentration, ligand concentration, and pressure). We monitored changes in the two-dimensional (2D) $\{^{1}H-^{15}N\}$ HSQC spectra of apo-NTnC upon lowering the temperature from 30 to 4 °C and determined the three-dimensional (3D) solution structure at 4 °C. Preliminary results of ^{15}N NMR relaxation measurements taken at 4 °C are also presented as Supporting Information. NMR and X-ray structures for apo-NTnC near ambient temperature (30 and 22 °C, respectively) were used for detailed comparisons to the structure at 4 °C.

EXPERIMENTAL PROCEDURES

Sample Preparation. The expression and purification of ^{15}N- and $^{15}N/^{13}C$-labeled NTnC (residues 1−90) was carried out as described previously (*32*). To accomplish decalcification of NTnC, 14 mg of the protein was dissolved in 0.5 mL of 100 mM EDTA and applied to a 1.5 cm × 90 cm G-25 gel filtration column, which was equilibrated with 25 mM NH_4HCO_3. The pooled fractions containing apo-NTnC were lyophilized, twice redissolved in water, and lyophilized again to ensure removal of NH_4HCO_3. Milli-Q deionized water was used in all steps. The NMR sample was prepared by dissolving 10 mg of apo-NTnC in 0.5 mL of H_2O containing 50 mM KCl, 10 mM EDTA, and 10% D_2O for spectrometer locking. The final pH of the sample was 6.7.

NMR Spectroscopy. All NMR spectra were obtained using Varian Unity INOVA 500 MHz or Unity 600 MHz NMR spectrometers equipped with triple-resonance probe heads and *z*-axis pulsed field gradients. All NMR spectra were acquired at 4 °C. The temperature was calibrated by monitoring the ^{1}H chemical shifts of methanol. Assignments of ^{1}H, ^{13}C (C_α and C_β), and ^{15}N resonances of apo-NTnC at 4 °C were carried out by acquiring the following sets of 2D and 3D NMR data: DQF-COSY (*33*), TOCSY (50 ms mixing time) (*34*), NOESY (25, 50, 75, 100, 125, and 150 ms mixing times) (*35*), $\{^{1}H-^{15}N\}$ HSQC (*36*), ^{15}N-filtered NOESY (50 ms mixing time) (*37*), ^{15}N-filtered TOCSY (75 ms mixing time) (*38*), and CBCA(CO)NNH (*39*). All spectra were acquired with the ^{1}H carrier centered at the water frequency (5.01 ppm), and water suppression was achieved by a low-power (20 Hz) water presaturation pulse 1.0−1.5 s in duration. The 3D ^{15}N-edited TOCSY and ^{15}N-edited NOESY spectra were recorded with spectral widths of 7000 (t_3) and 6500 Hz (t_1) for the direct and indirect ^{1}H dimensions, respectively, and 1600 Hz (t_2) for the ^{15}N dimension. A total of 512 complex points in t_3 (^{1}H) were collected with 164 t_1 (^{1}H) and 32 t_2 (^{15}N) increments. Resolution enhancement of these 3D experiments was accomplished by proper combinations of linear prediction (64 complex points in t_1 and 32 complex points in t_2), zero filling, and 60°-shifted sine-bell squared apodizations, to yield 3D spectra composed of 1024 (^{1}H) × 512 (^{1}H) × 64

(^{15}N) points. The 3D ^{15}N-edited HNHA spectra (*40*) were recorded with spectral widths of 6000 Hz (t_3) and 4500 Hz (t_1) for the direct and indirect ^{1}H dimensions, respectively, and 1500 Hz (t_2) for the ^{15}N dimension. A total of 384 complex points in t_3 (^{1}H) were collected with 80 t_1 (^{1}H) and 48 t_2 (^{15}N) increments. The data were resolution enhanced by zero filling, linear prediction (extension of t_1 by 40 complex points and t_2 by 24 complex points), and 60°-shifted sine-bell squared apodizations, which yield 3D spectra composed of 1024 (^{1}H) × 512 (^{1}H) × 128 (^{15}N) points. For all experiments, postacquisition solvent suppression by convolution of the time domain data was applied prior to Fourier transformation (*41*). All of the NMR data were processed and analyzed on a SGI Power Indigo2 workstation (Silicon Graphics, Mountain View, CA) using NMRPipe (*42*) and PIPP (*43*). The ^{1}H chemical shifts were referenced to the internal standard 2,2-dimethyl-2-silapentane-5-sulfonic acid (DSS). The ^{13}C and ^{15}N chemical shifts were indirectly referenced from DSS by using the frequency ratios: 0.251449539 for ^{13}C/^{1}H and 0.101329118 for ^{15}N/^{1}H (*44*).

Structural Determination. Interproton distance restraints were obtained from ^{15}N-filtered NOESY and simultaneous ^{15}N/^{13}C-filtered 3D NOESY experiments performed in H_2O. The mixing time dependence of the transient NOE was determined from 2D NOESY spectra at 4 °C to assess the effects of spin diffusion; subsequently, the mixing time was set to 50 ms for the NOESY experiments used to obtain experimental NOE restraints. The intensities of 2D and 3D NOESY data were calibrated on the basis of NOEs corresponding to a known distance such as Phe $H_\delta-H_\epsilon$ (2.48 Å), and an error of 50% was assumed for the NOE peak intensities. The following distance constraints were used to calibrate the 3D spectra: $HN_i-H_{\alpha i} = 2.70-3.05$ Å (for residues with negative ϕ values), $HN_i-H_{\alpha i-1} = 1.7-3.6$ Å, $H-C-C-H = 2.2-3.1$ Å, $H-C-CH_3 = 2.5-2.7$ Å, and $H-C-H = 1.7-1.8$ Å. In cases where direct calibration was not possible, the distance constraints were overestimated. For NOEs found only in 120 ms NOESY spectra, the upper bound was set to 6 Å. Dihedral angle restraints for the ϕ angle were estimated from the 3D HNHA experiment, using a correction factor of 1.1. A 25% error on the peak intensities was assumed, and the minimum ϕ angle restraint range was set to ±20°. The initial sets of restraints for the apo-NTnC structure at 4 °C contained no dihedral angle restraints and a fraction of the NOEs given in Table 1. These initial sets of restraints were used for calculating 100 starting structures from an extended conformation using the simulated annealing (SA) protocol in X-PLOR (*45*) with heating for 60 ps and cooling for 30 ps. Approximately 70% of the initial structures converged. The structure refinement was carried out starting with the 50 lowest-energy converged structures using the X-PLOR SA protocol with heating for 30 ps and cooling for 20 ps. The set of structures presented in this study includes the 40 lowest-energy structures selected from the 50 structures obtained in the last round of refinement.

Table 1: Statistics of the 40 Solution Structures of Apo-NTnC Determined at 4 °C[a]

no. of distance restraints	
total	1165
intraresidue	422
sequential ($\|i-j\| = 1$)	310
medium ($2 \le \|i-j\| \le 5$)	288
long ($\|i-j\| \ge 5$)	145
dihedral restraints (ϕ)	78
restraints violation	
distance (>0.05 Å)	10
dihedral (>2°)	0
rmsd (Å^2)	
well-defined regions[b]	
backbone atoms	0.46 ± 0.07
heavy atoms	0.97 ± 0.08
helix	0.27 ± 0.09
energies (kcal/mol)	
F_{total}	91.29 ± 0.31
F_{bonds}	1.32 ± 0.02
F_{angles}	75.03 ± 0.19
$F_{impropers}$	11.96 ± 0.02
$F_{van-der-Waals}$ (F repel)[c]	2.25 ± 0.02
F_{NOE}[d]	0.67 ± 0.03
$F_{dihedral}$[d]	0.07 ± 0.01
rmsd from experimental restraints	
NOE distance restraints (Å)	0.0034 ± 0.0001
dihedral angle restraints (deg)	0.1170 ± 0.0048
rmsd from ideal covalent geometry	
bonds (Å)	0.000986 ± 0.000008
angles (deg)	0.4492 ± 0.0006
impropers	0.3420 ± 0.0004
ϕ and φ in core and allowed regions (%)	99.0

[a] The number of each type of restraint used in the structure calculation is given in parentheses. None of the structures exhibit distance violations of >0.10 Å or dihedral violations of >2.0°. [b] Seventy-two percent of the backbone residues are well-defined, which includes residues 5−29, 36−48, 55−64, and 72−87. The averages of the backbone atom rmsds when each helix is separately superimposed onto its average are 0.34 ± 0.09 Å for N, 0.29 ± 0.09 Å for A, 0.26 ± 0.07 Å for B, 0.23 ± 0.09 Å for C, and 0.24 ± 0.06 Å for D. [c] The force constant for the van der Waals energy calculation was 4.0 kcal mol^{-1} Å^{-4}. [d] Force constants for the calculation of NOE and dihedral energies were 50 kcal mol^{-1} Å^{-2} and 200 kcal mol^{-1} rad^{-2}, respectively. ϕ and ψ dihedral angles in the core and allowed regions of the Ramachandran plot were determined by the program PROCHECK (*52*).

RESULTS

We have used changes in the 2D {^{1}H−^{15}N} HSQC NMR spectrum to follow the effect of temperature on the structure and dynamics of apo-NTnC. Figure 1 shows the superimposition of HSQC spectra of apo-NTnC acquired at 4 and 30 °C. Assignments are indicated for well-separated cross-peaks at 4 °C. The cross-peaks of Ser^2 and Met^3 are identified in the spectrum at 4 °C, whereas they were not identified at 30 °C, presumably due to rapid exchange with solvent. For most of the cross-peaks, the line widths do not appear to be significantly broadened by decreasing the temperature, primarily because of the application of resolution enhancement. However, the line width of an NMR peak is given by $\Delta\nu_{1/2} = 1/(\pi T_2)$ (in hertz), and the average ^{15}N T_2 for the backbone amides is decreased from 168 ± 7.5 ms at 30 °C (*29*) to 79 ± 0.7 ms at 4 °C. As indicated by the arrows in Figure 1, the positions of some of the cross-peaks assigned at 30 °C can easily be traced to their corresponding peaks at 4 °C, while for peaks in the congested area (7.5−8.5 ppm in the ^{1}H dimension), assignment is ambiguous. Hence, we have assigned the resonances of apo-NTnC at 4 °C on the basis of 2D and 3D NMR experiments. The backbone ^{15}N and $^1H_\alpha$ resonances of all residues except Ala^1 (presumably not present due to rapid exchange with solvent) were successfully assigned, and confirmed by correlation with the $^{13}C_\alpha$ and $^{13}C_\beta$ resonances through the CBCA(CO)NNH experiment. An example of the final assignment has been shown previously (strip plots from the ^{15}N-filtered NOESY

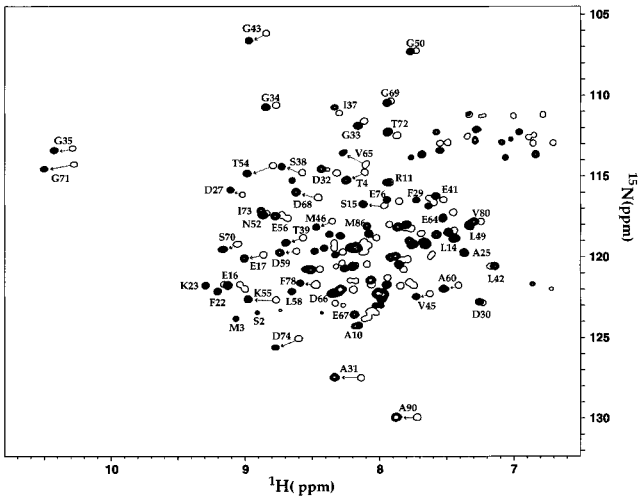

FIGURE 1: Superimposition of the 2D {^{15}N−^{1}H} HSQC spectrum of apo-NTnC acquired at 4 °C (filled cross-peaks) and at 30 °C (unfilled cross-peaks). Assignments are indicated for well-separated cross-peaks at 4 °C. Arrows indicate the direction of movement of well-separated cross-peaks upon lowering the temperature from 30 to 4 °C.

experiment) (*46*). The nearly complete assignment enables us to characterize in great detail the chemical shift changes of apo-NTnC upon decreasing the temperature from 30 to 4 °C.

As shown in Figure 1, most of the {^{1}H−^{15}N} HSQC cross-peaks shift slightly to lower field in both the ^{1}H (less than about 0.25 ppm) and ^{15}N (less than about 2.0 ppm) dimensions with decreasing temperatures. The NMR spectral changes are different from those which occur upon titration of NTnC with Ca^{2+} (see Figure 1 in ref *32*), where peaks are observed to undergo larger-magnitude shifts (compared to effects of decreasing temperature) of less than about 1.3 ppm for ^{1}H and less than about 14.0 ppm for ^{15}N. These chemical shift changes upon Ca^{2+} titration occur to both lower and higher fields for ^{1}H and ^{15}N.

For peptides, changes of the amide ^{1}H NMR chemical shift with temperature are linear and the slope gives the temperature coefficient ($-\delta\Delta_{NH}/\Delta T$) in parts per billion per kelvin, where $-\delta\Delta_{NH}$ is the difference of the NH chemical shift between 4 and 30 °C. The temperature coefficient is often taken as an empirical measure of the strength of hydrogen bonding (*47*, *48*). Figure 2a shows the temperature coefficients calculated for apo-NTnC. Interestingly, no correlation is observed between the temperature coefficients and the secondary structural elements of apo-NTnC, and many values are near the maximum value of about 10 ppb K^{-1}. These results support previous indications that the temperature coefficient is rarely correlated with the structure of a globular protein (*49*). Positive values for temperature coefficients are observed for seven amino acid residues (Gln^{7}, Ala^{8}, Ala^{25}, Leu^{42}, Leu^{49}, Glu^{76}, and Arg^{84}) as indicated in Figure 2a. These may be ascribed to local changes around the backbone amides of these amino acids. These amides may be influenced by changes in tertiary structure upon decreasing the temperature. Indeed, some of the above-mentioned residues are located close to aromatic residues (Phe^{22}, Phe^{26}, and Phe^{78}) which exhibit hydrophobic contacts with each other in apo-NTnC (*20*−*28*). It should be noted that Findlay and Sykes (*50*) and Tsuda et al. (*46*) reported significant line

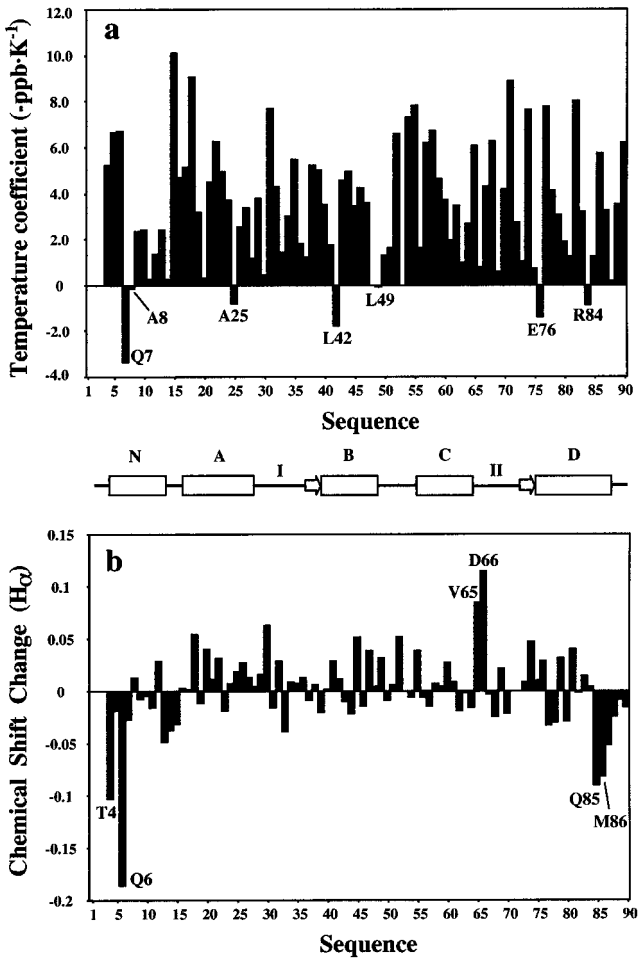

FIGURE 2: (a) Temperature coefficients (parts per billion per kelvin) for the backbone amide protons of chicken skeletal muscle NTnC. (b) Chemical shift changes (the difference between 30 and 4 °C) of the H_α resonances upon decreasing the temperature. The secondary structure of apo-NTnC is also shown, as well as Ca^{2+}-binding loops I and II. In panel b, the largest upfield chemical shift changes are observed for residues located at the N- and C-termini. The third largest downfield chemical shift change is observed for Val^{65} and Asp^{66}, which suggests an orientational change for helix C.

broadening for the δ-ring ^{1}H resonance of Phe^{26} when the temperature was decreased from 30 to 1 °C. This was ascribed to a reduction in the rate of ring-flipping motion, which is consistent with a view in which the environment surrounding Phe^{26} becomes more tightly packed, thereby increasing the barrier to flipping of aromatic side chains involved in the hydrophobic core of apo-NTnC.

The ^{1}H NMR chemical shift changes of the H_α proton resonances upon decreasing the temperature (the difference between 30 and 4 °C) is shown in Figure 2b. The largest negative values, corresponding to upfield shifts of the H_α resonances, are detected for residues located at the N- and C-termini. These changes can be attributed to a decrease in the rate of exchange with solvent and an increase in the level of helical secondary structure of these regions. The decrease in the rate of solvent exchange is correlated with changes in backbone amide ^{15}N NMR relaxation data between 30 (*29*) and 4 °C. For example, the order parameter (S^2) derived from ^{15}N relaxation data for Glu^{88} increases from 0.39 at 30 °C

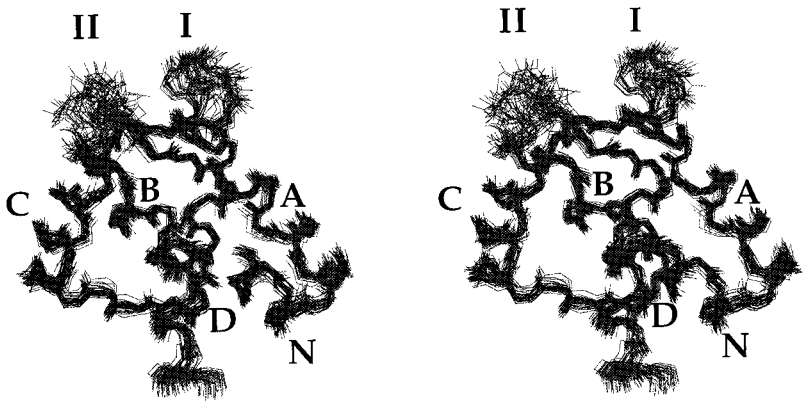

FIGURE 3: Stereoview of the solution structure of apo-NTnC at 4 °C. The backbone atoms (N, C_α, and C′) of the family of 40 structures are superimposed and displayed in the "rods" representation. α-Helices N (residues 3−13), A (residues 16−28), B (residues 39−48), C (residues 55−64), and D (residues 75−89) and the antiparallel β-sheet (residues 36−38 and 72−74) are well-defined. The linker (residues 49−54) and Ca^{2+}-binding sites I (residues 30−41) and II (residues 66−77) are less well-defined than the helices. Only residues 9−90 are shown to avoid congestion. The figure was produced with the programs Molscript (*59*) and Raster3D (*60*).

to 0.48 at 4 °C.[2] The upfield shifts of the H_α resonances are indicative of an increase in helicity for the N- and C-terminal helices, as determined using the criteria of the chemical shift index (CSI) (*51*). In addition, improved structural definition is evident on the basis of there being a larger number of interresidue NOE contacts for the N- and D-helices for apo-NTnC at 4 °C than at 30 °C. Large changes are also observed for the H_α resonances of Val^{65} and Asp^{66} which are located at the end of helix C. The ϕ dihedral angle of Val^{65} changes from −84° to −115° upon Ca^{2+} binding (*32*). Thus, a conformational change of the BC unit with respect to the NAD unit induced by lowering of the temperature is expected to affect the chemical shift of Val^{65} and its neighbors. Upon binding of Ca^{2+}, the ϕ angle for Glu^{41} changes from −96° to −65° as the BC unit moves away from the NAD unit (*32*). However, no significant change is detected for the H_α chemical shift of Glu^{41} upon lowering the temperature.

To elucidate detailed structural changes in apo-NTnC induced by lowering of the temperature, we have determined the 3D structure of apo-NTnC at 4 °C. The structure was calculated with 1243 experimental restraints derived from NMR, as listed in Table 1. Figure 3 shows a stereoview of the best fit superposition of the backbone atoms of the apo-NTnC structural ensemble at 4 °C. The apo-NTnC solution structure consists of five helices [residues 2−13 (N), 16−28 (A), 42−48 (B), 55−64 (C), and 75−89 (D)] and a short antiparallel β-sheet (residues 36−38 and 72−74) which connects Ca^{2+}-binding sites I (residues 30−41) and II (residues 66−77). These structural elements of apo-NTnC at 4 °C are the same as those identified in the previously determined 30 °C NMR structures (*24*). The five α-helices and the antiparallel β-sheet of apo-NTnC at 4 °C are well-defined with individual backbone root-mean-square deviations (rmsds) of 0.27 ± 0.09 Å for the helices and 0.13 ± 0.07 Å for the β-sheet. The structural quality at 4 °C is comparable to that of the recently reported $2Ca^{2+}$-E41A-NTnC structure at 30 °C which showed backbone rmsd values of 0.23 ± 0.07 Å for the α-helices and 0.25 ± 0.08 Å for the β-sheet (*26*). The structures of apo-NTnC at 4 °C and 2Ca-E41A-NTnC at 30 °C were determined on the basis of similar numbers of restraints and techniques. Interestingly, the backbone rmsd value for the N-helix decreases from 0.54 ± 0.06 Å at 30 °C to 0.34 ± 0.09 Å at 4 °C. The kink at Glu^{41} in the first half of helix B, as observed in the 30 °C NMR structure (*24*) and the crystal structure (*20*, *21*), is identified in the low-temperature structure by a large $^3J_{HNH\alpha}$ coupling constant determined during the 3D HNHA experiment. For Glu^{41}, a $^3J_{HNH\alpha}$ of 8.9 Hz is obtained, while values of <5.0 Hz are obtained for all other residues in helix B. Sites I and II are less well-defined than the helices, with rmsds of 0.70 ± 0.15 and 0.95 ± 0.36 Å, respectively. The poorer definition of the Ca^{2+}-binding sites compared to that of the helices is due in part to a smaller number of experimental restraints for the sites. Other poorly defined regions include the N- and C-termini, and the BC linker, although these regions are more well-defined compared to the 30 °C apo-NTnC NMR structure (*24*). ^{15}N relaxation measurements show that the order parameters (S^2) for the N- and C-termini, BC linker, and the Ca^{2+}-binding sites for apo-NTnC are lower than those for the other regions at 4 °C, as observed for apo-NTnC at 30 °C (*29*), indicating that the poorer definition of these regions is partly due to motional flexibility.[2]

The program PROCHECK (*52*) was used to determine the distribution of backbone dihedral angles. For all residues, 88% of the ϕ and ψ dihedral angles fell into the most favored region and 11% originate from glycines distributed within the additional allowed region.

In Figure 4a, the minimized average structure of apo-NTnC at 4 °C is compared with that determined at 30 °C (*24*). As shown in Figure 4a, the global fold of apo-NTnC at 4 °C is similar to that at 30 °C. In particular, the N−A, N−D, and A−D interhelical angles estimated for the NAD structural unit (residues 4−13, 16−28, and 75−87) are almost identical (Table 2). The structural invariance of the NAD unit upon Ca^{2+} binding (*26*, *30*) enables us to use this unit as a reference motif to determine detailed differences in structure between 30 and 4 °C. The backbone rmsd for the NAD unit for the 30 and 4 °C NMR structures is 1.73 ± 0.24 Å (Figure 4a). Interestingly, helix C of apo-NTnC at 4 °C is oriented more parallel to helix D by 30° compared to the 30 °C structure, indicating a tighter packing of the BC structural unit against the NAD unit at 4 °C. The C_α of Pro^{53}, the center

[2] S. Tsuda, S. M. Gagné, L. Spyracopoulos, and B. D. Sykes, unpublished data.

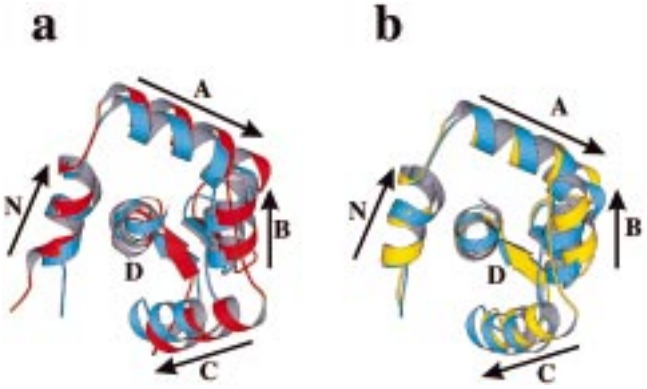

FIGURE 4: (a) Comparison of the structure of apo-NTnC at 4 °C with that of apo-NTnC at 30 °C (*24*), with the structures shown as blue and red ribbons, respectively. (b) Comparison of the structure of apo-NTnC at 4 °C with the X-ray structure of apo-NTnC at 22 °C (*20*), with the structures shown as blue and yellow ribbons, respectively. The NAD structural unit is superimposed in both panels a and b.

of the BC linker, moves 5 Å closer to the NAD unit at 4 °C compared to 30 °C. The direction of this movement is opposite to that of the Ca^{2+}-induced change where the BC linker moves 19 Å away from the NAD unit (*24*), suggesting that apo-NTnC undergoes a low-temperature-induced conformational "closing".

The low-temperature-induced conformational closing of apo-NTnC is characterized by a decrease of the accessible surface area of the nonpolar groups. If only residues 4−88 are considered, and using the Shrake definitions (*53*), the surface area of apo-NTnC for the 4 °C NMR structure is 2694 ± 63 and 3555 ± 88 Å^2 for the 30 °C NMR structure (*24*). The solution structure of apo-NTnC at 4 °C is more "closed" compared to the X-ray crystal structure (*21*). Figure 4b shows the 4 °C NMR structure and the X-ray crystal structure of apo-NTnC (*20*). It should be noted that crystal growth and data collection for the X-ray structure were performed at approximately 22 °C (M. N. G. James, personal communication). Like the comparison of the NMR structures at 4 and 30 °C, the arrangements of the NAD unit of the 4 °C NMR structure and 22 °C X-ray structures are virtually identical (Table 2), superimposing with a backbone rmsd of 0.53 ± 0.04 Å. As shown in Figure 4b, the BC structural unit moves toward the NAD unit, and the orientation of helix C of apo-NTnC at 4 °C becomes more parallel to helix D compared with the X-ray structure. This movement is quantified by a 10° increase in the interhelical angle between helices C and D (Table 2), and by 2 Å movement toward the NAD unit for the center of the BC linker. The accessible hydrophobic surface area of apo-NTnC at 4 °C is about 170 Å less than that for the crystal structure, which exposes 2866 Å^2 of the hydrophobic surface area for residues 4−88. These results show that apo-NTnC becomes more closed or compact upon lowering of the temperature.

DISCUSSION

The data presented here show for the first time detailed structural changes induced by low temperatures in apo-NTnC. The appearance of new peaks in the 2D $\{^1H-^{15}N\}$ HSQC spectrum at 4 °C originates from backbone amides in the N-helix (Ser^2 and Met^3), and line broadening for the ^1H δ resonances of the aromatic side chain of Phe^{26} in the hydrophobic core of apo-NTnC is a result indicative of a decrease in the rates of dynamical phenomena at the N-terminus and within the hydrophobic core. In addition, upfield shifts observed for H_α resonances of residues located within helices at the N- and C-termini are consistent with an increase in α-helical content, due in part to a decrease in dynamics at the ends of the molecule induced by lowering of the temperature. Furthermore, preliminary ^{15}N NMR relaxation data[2] indicate that the overall tumbling of apo-NTnC is slowed by a factor of 2 and the amplitude of internal motion at the N- and C-terminal helices is also decreased at 4 °C compared to that at 30 °C.

Significant downfield shifts of H_α resonances are detected for Val^{65} and Asp^{66} upon lowering of the temperature. Since Val^{65} has been known to be one of two hinges (Glu^{41} and Val^{65}) for the Ca^{2+}-induced opening of the BC unit (*24*), the observed change at Val65 is related to a reorientation of this unit. It should be noted that when NTnC undergoes a structural opening, the hinge at Val^{65} is straightened, and dihedral angles at this residue take values indicative of a strand upon Ca^{2+} binding. The hinge at the so-called B-helix kink (Glu^{41}) exhibits α-helical dihedral angles in the Ca^{2+}-saturated state (*24*, *26*).

In contrast to the calcium-induced structural change which involves an opening of NTnC, the low-temperature-induced structural change results in a closing of apo-NTnC. This is clearly demonstrated by the comparison of the present 4 °C NMR structure with both the 30 °C NMR structure (*24*) and the 22 °C X-ray structure (*20*) (Figure 4 and Table 2). Again, the downfield shift of H_α resonances of one of the hinge residues (Val^{65}) is thought to be supporting evidence of this closing (Figure 2). Although the NAD and BC units keep their respective structural motifs, lowering of the temperature induces a reduction of the distance between the two units, as quantified by a change in the interhelical angle between helices C and D, and a reduction in exposed hydrophobic surface area. Gagné et al. recently compared the C−D interhelical angle between currently available apo- and Ca^{2+}-bound TnC structures determined by either NMR or X-ray (*20*−*28*, *54*), each of which shows a different extent of opening for the BC unit. Interestingly, no pair of the above structures have the same C−D interhelical angle, differing even between the two X-ray structures of Ca^{2+}-bound rabbit skeletal muscle TnC in two different crystal forms (1TN4 and 2TN4) (*28*). Such differences can be explained by assuming that the BC unit is a flexible moeity. That is, the flexible BC unit falls into a different orientation having the lowest potential energy according to the sample conditions used, thus giving rise to different C−D interhelical angles between the crystal and solution structures (*59*). The C−D interhelical angle is highly sensitive to the orientational change of the BC unit. These observations are in accordance with these considerations; that is, the orientation of the BC unit can be changed as a function of temperature due to its dynamic nature.

The low-temperature-induced decrease in the rates dynamical phenomena and tighter packing of the BC unit against the NAD unit is related to the changes in the size of the internal cavity and extent of hydration of apo-NTnC. The partial specific volume of a molecule, $v°$, is a measure of the index of the cavity and extent of hydration. The temperature and/or pressure dependence of $v°$ has been

Table 2: Interhelical Angles of Structures of Apo-NTnC at 4 and 30 °C and in Crystal

	N−A (deg)	N−D (deg)	A−B (deg)	B−C (deg)	C−D (deg)	A−D (deg)
apo-NTnC at 4 °C (NMR)[a]	113 ± 2	63 ± 3	131 ± 3	129 ± 3	155 ± 3	110 ± 2
apo-NTnC at 30 °C (NMR)[b]	113 ± 3	68 ± 3	130 ± 3	126 ± 5	125 ± 4	111 ± 2
apo-NTnC in crystal (X-ray)[c]	116	62	134	125	145	116

[a] PDB file name 1SKT. [b] PDB file name 1TNP. [c] PDB file name 1TNQ.

estimated through measurements of adiabatic compressibility for a variety of proteins (*55*, *56*). The v° of a molecule at infinite dilution is described by a combination of the summation of the van der Waals volume of the component atoms (V_c), the volume of the cavity which originates from imperfections in atom packing (V_{cav}), and the change of the solution volume due to hydration of the protein (ΔV_{sol}):

$$v^\circ = V_c + V_{cav} + \Delta V_{sol} \quad (1)$$

The temperature derivative of v° is given by

$$\partial(v^\circ)/\partial(T) = \partial(V_{cav})/\partial(T) + \partial(\Delta V_{sol})/\partial(T) \quad (2)$$

where T is the absolute temperature. In the case of bovine serum albumin, v° changes from a value of 0.743 mL/g at 40 °C to 0.730 mL/g at 10 °C. This change was attributed to a decrease in the volume of the cavity, the first term of the right-hand side of eq 2, and an increase in the extent of hydration, the second term in eq 2 (note that ΔV_{sol} is negative) (*56*). In the case of apo-NTnC, a total volume of 10 889 Å^3 is estimated for the 22 °C X-ray structure and 10 645 Å^3 for the 4 °C NMR structure, assuming apo-NTnC is spherical in shape and considering only residues 4−88 [program VADAR, D. S. Wishart et al., University of Alberta, Edmonton, AB (*57*)]. We can estimate the cavity volume to be approximately 2−5% of the total volume of a globular protein (*58*). Hence, the observed decrease of the hydrophobic surface from 2866 Å^2 at 22 °C to 2694 Å^2 at 4 °C is likely due to a decrease in the cavity volume induced by lowering the temperature. Further, our preliminary ^{15}N relaxation data[2] show that the overall rotational correlation time of apo-NTnC at 4 °C is 10.7 ± 0.2 ns, which is 2-fold slower than that the value of 4.9 ± 0.2 ns at 30 °C (*29*). The increase in the overall correlation time is consistent with the expected 2-fold increase in the viscosity of water from about 4 to 30 °C. Overall, the structural changes of apo-NTnC are consistent with a low-temperature-induced decrease in v°, as proposed on the basis of compressibility experiments.

A recent fluorescence study by Foguel et al. (*31*) with a tryptophan mutant apo-NTnC (F29W) proposed that low temperature (−11 °C) and high pressure (2.2 kbar) cause a structural change similar to the Ca^{2+}-induced structural opening at normal temperature and pressure. Additionally, the change in fluorescence intensity was observed to be small when temperature alone is decreased at atmospheric pressure (*31*). It should be noted that low temperature alone and low temperature with high pressure are expected to have different effects on the compressibility and partial specific volume of a protein (*55*). Over the temperature range evaluated in this study (4−30 °C), the pressure was atmospheric (1 bar), and we did not observe an open conformation, analogous to the Ca^{2+}-saturated state, for apo-NTnC. Therefore, we feel that the dominant factor which induces changes in the fluorescence data of apo-NTnC is high pressure, and not low temperature.

The packing of the BC unit of apo-NTnC onto the NAD structural unit buries hydrophobic side chains that make up the hydrophobic surface of the regulatory domain which is exposed upon Ca^{2+} binding (*24*). The burial of the hydrophobic surface alters the interaction between TnC and TnI, an event which is believed to be a key factor for the inactivation of muscle contraction. The exposure of the hydrophobic pocket of the regulatory domain of TnC upon Ca^{2+} binding is commensurate with muscle contraction (*1*−*4*). A reduction in temperature causes a decrease in the exposed hydrophobic surface area in the apo state. Thus, part of the larger energetic cost of opening NTnC at lower temperatures is the need to expose a more tightly packed hydrophobic core; i.e., the Ca^{2+}-induced opening in NTnC requires more activation energy at low temperatures. If this hypothesis is correct, it provides insight into the design of an efficient cold-adapted NTnC that opens more readily at lower temperatures in response to Ca^{2+}. The mutant protein could include changes around Val^{65} that would restrict the packing of the BC unit onto the NAD unit, and perhaps more methionine residues in the hydrophobic core of the protein. Recently, it has been proposed that the energetic cost of exposing buried methionines may be offset by favorable gains in entropy (*29*). We are hopeful that the growing biological importance of the muscle regulatory proteins will provide exact knowledge about the low-temperature influence on the activation efficiency in contraction, which will support, refute, or require modification of the above suggested ideas.

ACKNOWLEDGMENT

We are very grateful to L. E. Kay for providing pulse sequences, M. X. Li and L. B. Smillie for assistance with sample preparation, G. McQuaid for keeping the spectrometer at optimum performance, and Mission Control (J. L. Willard, T. Jellard, and R. Boyko) for computer expertise.

SUPPORTING INFORMATION AVAILABLE

One table showing chemical shifts of the ^{1}H, ^{13}C, and ^{15}N resonances of chicken skeletal muscle troponin C in the Ca^{2+}-free state at pH 6.7 and 4 °C (Table S1). This material is available free of charge via the Internet at http://pubs.acs.org.

REFERENCES

1. Farah, C. S., and Reinach, F. C. (1995) *FASEB J. 9*, 755−767.
2. Leavis, P. C., and Gergely, J. (1984) *CRC Crit. Rev. Biochem. 16*, 235−503.
3. Zot, A. S., and Potter, J. D. (1987) *Annu. Rev. Biophys. Biophys. Chem. 16*, 535−559.
4. Grabarek, Z., Tao, T., and Gergely, J. (1992) *J. Muscle Res. Cell. Motil. 13*, 383−393.

5. Strynadka, N. C. J., and James, M. N. G. (1989) *Annu. Rev. Biochem. 58*, 951−998.
6. Romero-Herrera, A. E., Castillo, O., and Lehmann, H. (1976) *J. Mol. Evol. 8*, 251−270.
7. Collins, J. H., Potter, J. D., Horn, M. J., Wilshire, G., and Jackman, N. (1973) *FEBS Lett. 36*, 268−272.
8. Wilkinson, J. M. (1976) *FEBS Lett. 70*, 254−256.
9. van Eerd, J. P., Capony, J. P., Ferraz, C., and Pechere, J. F. (1978) *Eur. J. Biochem. 91*, 231−242.
10. Malencik, D. A., Heizmann, C. W., and Fischer, E. H. (1975) *Biochemistry 14*, 715−721.
11. Takagi, T., and Konishi, K. (1983) *J. Biochem. (Tokyo) 94*, 1753−1760.
12. Garone, L., Theibert, J. L., Miegel, A., Maeda, Y., Murphy, C., and Collins, J. H. (1991) *Arch. Biochem. Biophys. 291*, 89−91.
13. Kobayashi, T., Takagi, T., Konishi, K., and Wnuk, W. (1989) *J. Biol. Chem. 264*, 18247−18259.
14. Collins, J. H., Theibert, J. L., Francois, J. M., Ashley, C. C., and Potter, J. D. (1991) *Biochemistry 30*, 702−707.
15. Bullard, B., Dabrowska, R., and Winkelman, L. (1973) *Biochem. J. 135*, 277−286.
16. Kobayashi, T., Kagami, O., Takagi, T., and Konishi, K. (1989) *J. Biochem. (Tokyo) 105*, 823−828.
17. Ojima, T., Tanaka, H., and Nishita, K. (1994) *Arch. Biochem. Biophys. 311*, 272−276.
18. Obinata, T. (1988) in *Protein Nucleic Acid and Enzyme* (Endo, M., Nisizuka, Y., Yagi, K., and Miyamoto, E., Eds.) Vol. 33, pp 2033−2042, Kyoritsu Press, Tokyo, Japan.
19. Margesin, R., and Schinner, F. (1994) *J. Biotechnol. 33*, 1−14.
20. Herzberg, O., and James, M. N. G. (1988) *J. Mol. Biol. 203*, 761−779.
21. Satyshur, K. A., Rao, S. T., Pyzalska, D., Drendal, W., Greaser, M., and Sundralingham, M. (1988) *J. Biol. Chem. 263*, 1628−1647.
22. Herzberg, O., Moult, J., and James, M. N. G. (1986) *J. Biol. Chem. 261*, 2638−2644.
23. Findlay, W. A., Sönichssen, F. D., and Sykes, B. D. (1994) *J. Biol. Chem. 269*, 6773−6778.
24. Gagné, S. M., Tsuda, S., Li, M. X., Smillie, L. B., and Sykes, B. D. (1995) *Nat. Struct. Biol. 2*, 784−789.
25. Slupsky, C. M., and Sykes, B. D. (1995) *Biochemistry 34*, 15953−15964.
26. Gagné, S. M., Li, M. X., and Sykes, B. D. (1997) *Biochemistry 36*, 4386−4392.
27. Strynadka, N. C. J., Chernaia, M., Sielecki, A. R., Li, M. X., Smillie, L. B., and James, M. N. G. (1997) *J. Mol. Biol. 273*, 238−255.
28. Houdusse, A., Love, M. L., Dominguez, R., Grabarek, Z., and Cohen, C. (1997) *Structure 5*, 1695−1711.
29. Gagné, S. M., Tsuda, S., Spyracopoulos, L., Kay, L. E., and Sykes, B. D. (1998) *J. Mol. Biol. 278*, 667−686.
30. Spyracopoulos, L., Li, M. X., Sia, S. K., Gagné, S. M., Chandra, M., Solaro, J., and Sykes, B. D. (1997) *Biochemistry 36*, 12138−12146.
31. Foguel, D., Suarez, M. C., Barbosa, C., Rodrigues, J. J., Jr., Sorenson, M. M., Smillie, L. B., and Silva, J. L. (1996) *Proc. Natl. Acad. Sci. U.S.A. 93*, 10642−10646.
32. Gagné, S. M., Tsuda, S., Li, M. X., Chandra, M., Smillie, L. B., and Sykes, B. D. (1994) *Protein Sci. 3*, 1961−1974.
33. Rance, M., Sørensen, O. W., Bodenhausen, G., Wagner, G., Ernst, R. R., and Wüthrich, K. (1983) *Biochem. Biophys. Res. Commun. 117*, 479−485.
34. Braunschweiler, L., and Ernst, R. R. (1983) *J. Magn. Reson. 53*, 521−528.
35. Jeener, J., Meier, B. H., Bachmann, P., and Ernst, R. R. (1979) *J. Chem. Phys. 71*, 4546−4553.
36. Palmer, A. G., III, Cavanagh, J., Wright, P. E., and Rance, M. (1991) *J. Magn. Reson. 93*, 151−170.
37. Kay, L. E., Marion, D., and Bax, A. (1989) *J. Magn. Reson. 84*, 72−84.
38. Marion, D., Driscoll, P. C., Kay, L. E., Wingfield, P. T., Bax, A., Gronenborn, A. M., and Clore, G. M. (1989) *Biochemistry 28*, 6150−6156.
39. Muhandiram, D. R., and Kay, L. E. (1994) *J. Magn. Reson. 103*, 203−216.
40. Kuboniwa, H., Grzesiek, S., Delaglio, F., and Bax, A. (1995) *J. Biomol. NMR 4*, 871−878.
41. Marion, D., Ikura, M., and Bax, A. (1989) *J. Magn. Reson. 84*, 425−430.
42. Delaglio, F., Grzesiek, S., Vuister, G. W., Zhu, G., Pfeifer, J., and Bax, A. (1995) *J. Biomol. NMR 6*, 277−293.
43. Garrett, D. S., Powers, R., Gronenbom, A. M., and Clore, G. M. (1991) *J. Magn. Reson. 95*, 214−220.
44. Wishart, D. S., Bigam, C. G., Yao, J., Abildgaard, F., Dyson, H. J., Oldfield, E., Markley, J. L., and Sykes, B. D. (1995) *J. Biomol. NMR 6*, 135−140.
45. Brünger, A. T. (1992) *X-PLOR Version 3.1: A System for X-ray Crystallography and NMR*, Yale University Press, New Haven, CT.
46. Tsuda, S., Gagné, S. M., and Sykes, B. D. (1996) in *35th Experimental NMR conference in Japan*, November 21, 1996, Kyoto, Japan, pp 249−252 (abstract).
47. Deslauriers, R., and Smith, I. C. P. (1980) in *Biological Magnetic Resonance* (Berliner, L. J., and Reuben, J., Eds.) Vol. 2, pp 243−344, Plenum Press, New York.
48. Baxter, N. J., and Williamson, M. P. (1997) *J. Biomol. NMR 9*, 359−369.
49. Evans, J. N. S. (1995) *Biomolecular NMR Spectoscopy*, Oxford University Press, New York.
50. Findlay, W. A., and Sykes, B. D. (1993) *Biochemistry 32*, 3461−3467.
51. Wishart, D. S., Sykes, B. D., and Richard, F. M. (1991) *J. Mol. Biol. 222*, 311−333.
52. Laskowski, R. A., MacArthur, M. W., Moss, D. S., and Thorton, J. M. (1993) *J. Appl. Crystallogr. 26*, 283−290.
53. Shrake, A., and Rupley, J. A. (1973) *J. Mol. Biol. 79*, 351−371.
54. Gagné, S. M., Spyracopoulos, L., McKay, R. T., Sykes, M. T., Tsuda, S., Kay, L. E., and Sykes, B. D. (1998) in *XVIIIth International Conference on Magnetic Resonance in Biological System*, August 25, 1998, Tokyo, Japan, p 54.
55. Iqbal, M., and Verrall, R. E. (1987) *J. Phys. Chem. 91*, 1935−1941.
56. Gekko, K., and Hasegawa, Y. (1989) *J. Phys. Chem. 93*, 426−429.
57. Wishart, D. S., Willard, L., Richards, F. M., and Sykes, B. D. (1994) *VADAR: A comprehensive program for protein structural evaluation*, version 1.2, University of Alberta, Edmonton, AB.
58. Rashin, A. A., Iofin, M., and Honig, B. (1986) *Biochemistry 25*, 3619−3625.
59. Kraulis, P. J. (1991) *J. Appl. Crystallogr. 24*, 946−950.
60. Merritt, E. A., and Murphy, E. P. M. (1994) *Acta Crystallogr. D50*, 869−873.

BI982936E